Experimental Verification of Overlimiting Current by Surface Conduction and Electro-Osmotic Flow in Microchannels

Sungmin Nam,[1,‡] Inhee Cho,[1] Joonseong Heo,[2] Geunbae Lim,[2] Martin Z. Bazant,[3] Dustin Jaesuk Moon,[1] Gun Yong Sung,[4,*] and Sung Jae Kim[1,5,†]

[1]*Department of Electrical and Computer Engineering, Seoul National University, Seoul 151-744, Republic of Korea*
[2]*Department of Mechanical Engineering, Pohang University of Science and Technology, Pohang 790-784, Republic of Korea*
[3]*Department of Chemical Engineering and Mathematics, Massachusetts Institute of Technology, Cambridge, Massachusetts 02139, USA*
[4]*Department of Material Science and Engineering, Hallym University, Chunchon 200-702, Republic of Korea*
[5]*Big Data Institute and Inter-university Semiconductor Research Center, Seoul National University, Seoul 151-744, Republic of Korea*

(Received 16 July 2013; revised manuscript received 9 September 2014; published 16 March 2015)

Direct evidence is provided for the transition from surface conduction (SC) to electro-osmotic flow (EOF) above a critical channel depth (d) of a nanofluidic device. The dependence of the overlimiting conductance (OLC) on d is consistent with theoretical predictions, scaling as d^{-1} for SC and $d^{4/5}$ for EOF with a minimum around $d = 8$ μm. The propagation of transient deionization shocks is also visualized, revealing complex patterns of EOF vortices and unstable convection with increasing d. This unified picture of surface-driven OLC can guide further advances in electrokinetic theory, as well as engineering applications of ion concentration polarization in microfluidics and porous media.

DOI: 10.1103/PhysRevLett.114.114501 PACS numbers: 47.61.Fg, 85.85.+j, 87.85.Rs

Over the past decade, electrokinetic phenomena inside nanoscale fluidic channels have drawn significant attention for developing both fundamental theory and novel engineering applications [1–6]. Noticeable progress has been made in understanding electroconvection during ion concentration polarization (ICP) due to electro-osmotic flows near the membrane or nanochannel interface driving salt depletion [5,7–10]. Due to the complexity of direct numerical simulation of the Poisson equation (for electric potential), Nernst-Planck equations (for ion concentrations), and Navier-Stokes equations (for fluid flows) in multidimensional geometries [9,11,12], as well as inherent limitations of the classical dilute solution model [13], it is crucial to directly observe particle motions and flow fields in precisely controlled micro- or nanofluidic geometries [14,15].

Recent experimental investigations based on the micro- or nanofluidic platform reveal complex electrokinetic phenomena in microchannels near an ion permselective membrane or nanochannel junctions, which cannot be described by one-dimensional diffusion-drift equations. The classical theory of ICP predicts a constant concentration gradient in the quasineutral electrolyte and saturation of the current to the Nernst diffusion-limited value at high voltage [16]. The key features of steady ICP under dc bias are as follows. (1) In case of a cation selective membrane, the electrolyte concentration at the anodic side of the membrane is nearly depleted within the ICP layer and approaches zero adjacent to the membrane at the limiting current [17]. (2) Due to the low salt concentration, the electrical conductivity significantly decreases, leading to a greatly amplified local electric field [18]. (3) The large electric field drives fast electrokinetic flow inside the depletion zone leading to strong vortices in order to satisfy the continuity conditions [19,20]. (4) The strongest vortex at the membrane leads to secondary vortices to form a stepwise concentration profile inside the depletion zone, providing inherent instability issues [21–23]. (5) The limiting current and overlimiting conductance (OLC) can be adjusted by manipulating the strong convection [8,24]. Since the ion depletion zone expands with the strong convection, suppressing the convection can reduce the total electrical resistance of the system, but the opposite trend is also possible since electroconvection clearly lowers the resistance close to the limiting current and compensates for the reduced conductivity. The dependence of these competing effects on voltage and geometry remains to be fully understood. (6) The salt concentration tends to form very sharp gradients between the depleted and concentrated regions (on the anodic, depleted side of the membrane), perhaps first observed a decade ago [25]. In micro-nanofluidic device in which steady over-limiting current has been observed [26], salt gradients propagate as shock waves, [6,27] or "deionization shocks" [28–30] at constant current, due to the nonlinear effect of ion transport in the electric double layers of the sidewalls. These observations suggest that multiple transport mechanisms may be involved when overlimiting current occurs under strong confinement.

A unified scaling theory of OLC through an electrolyte confined within a charged microchannel has recently been developed [31,32], but direct experimental confirmation is

still lacking. The theory predicts a transition between two new mechanisms, surface conduction (SC) and electro-osmotic flow (EOF), that dominate in nanochannels and microchannels, respectively. The EOF mechanism is driven by large electro-osmotic slip in the depleted region on the sidewalls (not the membrane at the end of the channel) [33], leading to "wall fingers" of salt transported by vortices faster than transverse diffusion [31,34]. This new mode of surface convection thus cannot be described by classical Taylor-Aris dispersion [33,34]. The EOF mechanism, extended for "eddy fingers" in a random porous medium, has been confirmed indirectly by experiments measuring the current-voltage relation, scaling with salt concentration or surface charge, and desalination efficiency of "shock electrodialysis" [35]. The SC mechanism has also been confirmed in straight nanopores with controlled surface charge by again predicting the current-voltage relation and by *ex situ* imaging of metal electrodeposits grown along the pore walls by SC [36]. However, no theory or experiment has shed light on the roles of SC and EOF during transient deionization shock propagation, and several assumptions of the steady-state scaling theory have been called into question by direct numerical simulations [32].

In this Letter, we provide the first *in situ* observation of the SC and EOF mechanisms for overlimiting current and deionization shock propagation, and their dependence on geometrical confinement. The motion of fluorescent tracer particles is visualized to reveal the internal dynamics in both regimes. The OLC is also measured, and the predicted scaling with channel depth is confirmed, including a minimum OLC that had escaped notice at the critical depth of the transition.

Micro- or nanofluidic devices are fabricated by a surface patterning method [37] in a poly-dimethyl siloxane substrate as shown in Fig. 1. Current is driven in aqueous 1 mM KCl solution through a cation permselective Nafion nanojunction to generate ICP. Under the experimental conditions, the surface charge of the poly-dimethyl siloxane microchannel is negative, as expected, since EOF is observed to be flowing toward the cathode. Each device has the same Ohmic conductance by fixing the cross-sectional area, while the depth is varied. The physical dimensions are shown in Table I. According to the theory using the typical surface charge of 50 mC in aqueous solution [31], the dominant mechanism of driving overlimiting current should vary with the microchannel depth among SC for $d < 8$ μm, electro-osmotic surface convection for 8 μm $< d <$ 400 μm, and electro-osmotic instability on the membrane for $d > 400$ μm. The quasisteady current-voltage relation is measured by linear sweep voltammetry with a slow sweep rate at 0.2 V/15 sec from 0 to 7 V, which is slow enough to avoid any overshoot of the limiting current signifying transient effects [35,38]. A customized LabView program automatically records the current data at each step. (See the Supplemental Material for experimental details [39].)

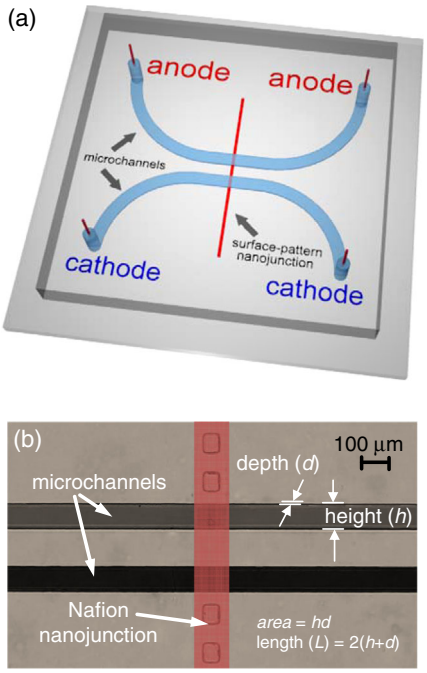

FIG. 1 (color online). Schematic diagrams of (a) an H-shaped micro- or nanofluidic device and (b) a microscope image of the device. External electric voltages are applied at two north reservoirs, while two south reservoirs are electrically grounded. The depth d and height h are varying to obtain the same cross-sectional area ($A = hd$).

Below the limiting current, as expected, the current-voltage relations of the microchannels with different depths all collapse onto a linear relationship, as shown in Fig. 2, indicated by "range (i)." The curves of 2, 6.5, 14.5, and 22 μm are only shown for graphical simplicity. We refer to this as the "Ohmic region" since there is a constant apparent conductivity for steady electrodiffusion, even though both diffusion and electromigration of the cations contribute to the total flux [16]. As the salt concentration approaches zero at the membrane interface, the classical diffusion limited current is reached, as indicated by "range (ii)" in Fig. 2. As the applied voltage increases further, another

TABLE I. Physical dimensions of a micro- or nanofluidic device of the same cross-sectional area.

d (μm)	h (μm)	*Area* (μm^2)	L (μm)
2	210	420	424
5	84	420	178
6.5	60	390	133
11	38	418	98
14.5	30	435	89
18	23	414	82
22	20	440	84

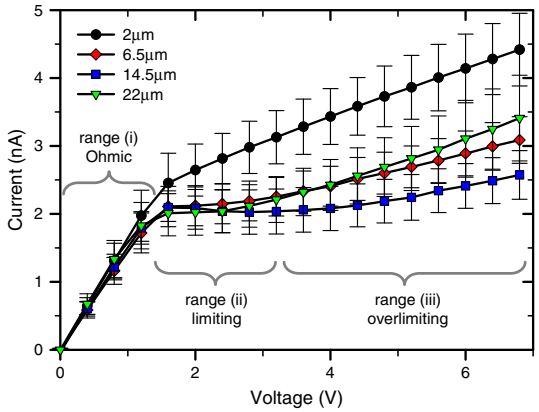

FIG. 2 (color online). Current-voltage relations for micro- or nanofluidic devices with varying h and d, but fixed cross-sectional area and thus fixed Ohmic conductance. As a result the conductance is constant for all devices below the limiting current, while limiting and overlimiting current values are significantly different. Voltage is swept at 0.2 V/15 sec. Each line is measured at least ten times for experimental repeatability.

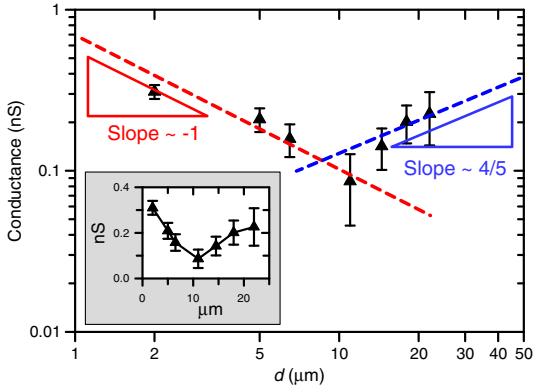

FIG. 3 (color online). OLC as a function of the microchannel depth in log-log scale. A linear scaled plot is shown in the inset. The data are consistent with the predicted transition from surface conduction ($\propto d^{-1}$) to electro-osmotic surface convection ($\propto d^{4/5}$) as the dominant transport mechanism.

region of overlimiting current with a constant and smaller conductance than Ohmic conductance is observed [range (iii)], whose physical origin should be determined. The trend with depth is qualitatively similar to the theoretical predictions [31]. For the thinnest channel (2 μm), the limiting current range is almost missing, and the OLC (slope) is the largest among all depths. Moreover, the 2 μm depth leads to the largest overlimiting current, since it has the largest surface area to volume ratio, experiencing the greatest effect of the new surface transport mechanisms.

In order to extract a quantitative conclusion, the OLC for each depth is obtained by linear regression of the slope of the data in range (iii) and plotted in log-log scale as shown in Fig. 3. The error bars increase in the deeper microchannels due to the flow instability, as clarified in the inset of Fig. 3. While previous studies have established the simple power-law scaling of OLC with salt concentration and surface charge in a fixed geometry [35,36], our data reveal a nonmonotonic dependence on the microchannel depth with a minimum conductance at a depth of roughly 8 μm. From previous theory [31,35], the OLC due to SC is proportional to the volume-area ratio, or inverse of depth, d^{-1}, in nanochannels and thus the OLC decreases with increasing depth. In contrast, the OLC due to electro-osmotic surface convection in microchannels is predicted to have the opposite trend, scaling as $d^{4/5}$. Although the 4/5 exponent follows from subtle scaling arguments [31,35], the increasing conductance with increasing depth can be easily understood as a result of larger vortices carrying more convective flux, i.e., thicker wall fingers.

The theoretical scaling is consistent with the "V-shaped" data in Fig. 3. The decreasing d^{-1} scaling for the thinner microchannels is clear from the data and supports the SC theory. The increasing $d^{4/5}$ scaling for EOF is also consistent with the data for the thicker microchannels as a possible limiting scaling law, although the data are not conclusive. Since direct numerical simulations have recently called some assumptions of the scaling theory into question [32], our data can guide further theoretical developments. Remarkably, however, the minimum conductance around $d = 8$ μm is identical to the theoretical prediction of the critical depth from the intersection of the two scaling laws [31]. According to the scaling theory, the critical depth depends weakly on most parameters (permittivity, viscosity, diffusivity, and temperature), but could in principle be tuned by varying the salt concentration c_0 as $d_c \sim [q_s(c_0)]^{1/3} c_0^{-4/9}$, and thus also the surface charge density $q_s(c_0)$ (via pH) [35].

In order to correlate the scaling transition in OLC with the existence of electroconvection, transient electrokinetic flows (not yet predicted by any theory) are imaged during the current-voltage measurement, and their snapshots are shown in Fig. 4. Each column has the same depth, and each row represents the time evolution of the flow field. Note that the scale bar in the first column is different from the others since the 2 μm deep device has a larger region of interest than the others. The electrolyte contains a fluorescent dye and microparticles to track both concentration and flow fields, respectively, as in previous work [19,21,37,40]. The microbeads clearly reveal convection and flow topology, although they can deviate from streamlines due to finite size effects (in small channels) and electrodiffusiophoresis (in large fields, near stagnation) [41]. The length of the depletion zone is also tracked by the dye, and it presumably represents the thickness of diffusive layer. (See the Supplemental Material [39].)

As shown in snapshots at 280s in Fig. 4, electrokinetic flow patterns are significantly different as a function of the depth of the microchannel. The details of the changes can be found in the videos in the Supplemental Material [39] for each depth. At 2 μm depth, a flat depletion zone propagates

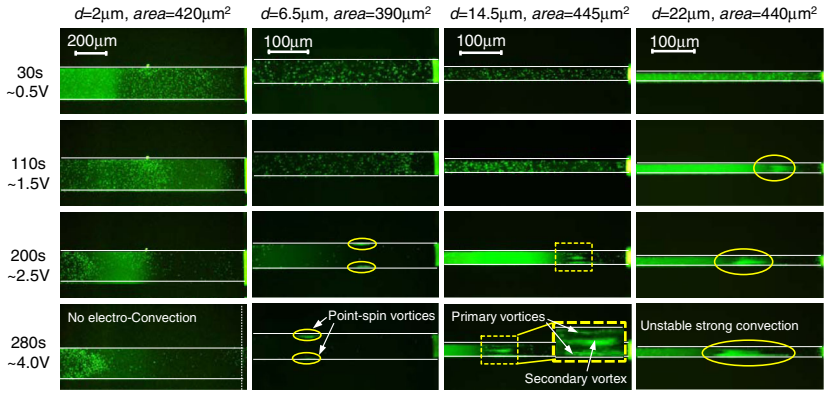

FIG. 4 (color online). Microscopic images of flow tracking by fluorescent dye and particles. Each image is taken at a given time (or voltage) as noted. Note that the scale bars are different. A shallow depth effectively suppresses electro-convective flow more than a deep one. At $d = 14.5$ μm, the convective flow at the top and bottom creates a secondary vortical flow at the stagnation point in the middle of the channel. Over $d = 22$ μm, the flow finally becomes unstable. See the videos in the Supplemental Material [39].

as a deionization shock wave from the nanojunction over the microchannel [6,25,27–30], and the strong vortical motions are largely suppressed and hardly observed because of geometrical constrictions [19,26]. Transverse diffusion of the dye across the depth also eliminates concentration gradients [31,34]. A pair of pointlike weak vortices is initiated at the top and bottom of the microchannel as shown in the case of the 6.5 μm deep microchannel (close to the transition depth of 8 μm), especially after the limiting current voltage of 2.5 V. As the depth increases to 14.5 μm, the larger vortices become the primary convections at the side of microchannel, while they induce secondary vortices at the stagnation point in the middle of the microchannel, leading to a strong electroconvective flow [21]. Finally, the electroconvection becomes very strong and unstable in case of the 22 μm deep microchannel, but still occurs behind the shock away from the membrane surface. Although this unstable flow resembles the bulk behavior [6,13,28–30], the channel is not nearly thick enough to see the Rubinstein-Zaltzman electro-osmotic instability, which originates on the membrane and is predicted to dominate only above 400 μm depth [31]. Combining the results of OLC measurement and the flow field tracking (e.g., the transition from the surface conduction governed regime to the electroconvection governed regime), we can suggest that the mechanism of overlimiting current behavior cannot be attributed solely to surface conduction or electro-osmotic surface or bulk convection. Instead, each phenomenon plays an important role and dominates in different micro- or nanochannel geometries, in ways not fully captured by existing models.

In summary, we experimentally demonstrate the competition between different transport mechanisms for overlimiting current in microchannels by fixing (or changing, see the Supplemental Material [39]) the Ohmic conductance. With the microscopic imaging of electrokinetic flow and electrical measurements, we can separate the effects of the EOF and SC depending on the geometrical confinement. Consistent with the theory [31,32], surface conduction dominates in shallow micro (or nano) channels and electroosmotic surface convection dominates in microchannels with a minimum OLC at the predicted transition around 8 μm depth, but the theory fails to predict complex EOF vortices and unstable convection, as the channel depth is increased further. Millimeter scale fluidic experiments, which are quite far from the geometrical range of the present work, should be required for detailed characterization of the electro-osmotic instability as suggested by Ref. [31]. Instead, present micro-nanofluidic platform has an effective confinement for suppressing this undesirable instability. A clear understanding of the mechanisms for overlimiting current in microchannels and porous media would be essential, not only to advance theoretical physics, but also to guide the engineering of ICP-based electrochemical systems, such as fuel cells, batteries, electrodesalination systems [2,7,8], and template-assisted electrodeposition [36].

This work is supported by the Basic Science Research Program (Grant No. 2013R1A1A1008125), by the Center for Integrated Smart Sensor funded as the Global Frontier Project (Grant No. CISS-2011-0031870), by the Future Based Technology Development Program (Nano Fields) (Grant No. 2012-0001033), and by the Ministry of Science, ICT & Future Planning and Korean Health Technology RND Project, Ministry of Health and Welfare of the Republic of Korea (Grants No. HI13C1468 and No. HI14C0559). S. N. and I. C. contributed equally to this work.

*Corresponding author.
gysung@hallym.ac.kr
†Corresponding author.
gates@snu.ac.kr
‡Present address: Department of Mechanical Engineering, Stanford University, Stanford, California 94305, USA.

[1] S. J. Kim, Y.-A. Song, and J. Han, Chem. Soc. Rev. **39**, 912 (2010).
[2] S. J. Kim, S. H. Ko, K. H. Kang, and J. Han, Nat. Nanotechnol. **5**, 297 (2010).
[3] H. Daiguji, Chem. Soc. Rev. **39**, 901 (2010).
[4] L. J. Cheng and L. J. Guo, Chem. Soc. Rev. **39**, 923 (2010).
[5] H. C. Chang, G. Yossifon, and E. A. Demekhin, Annu. Rev. Fluid Mech. **44**, 401 (2012).
[6] T. A. Zangle, A. Mani, and J. G. Santiago, Chem. Soc. Rev. **39**, 1014 (2010).
[7] V. V. Nikonenko, A. V. Kovalenko, M. K. Urtenov, N. D. Pismenskaya, J. Han, P. Sistat, and G. Pourcelly, Desalination **342**, 85 (2014).
[8] V. V. Nikonenko, N. D. Pismenskaya, E. I. Belova, P. Sistat, P. Huguet, G. Pourcelly, and C. Larchet, Adv. Colloid Interface Sci. **160**, 101 (2010).
[9] C. L. Druzgalski, M. B. Andersen, and A. Mani, Phys. Fluids **25**, 110804 (2013).
[10] B. Zaltzman and I. Rubinstein, J. Fluid Mech. **579**, 173 (2007).
[11] M. K. Urtenov, A. M. Uzdenova, A. V. Kovalenko, V. V. Nikonenko, N. D. Pismenskaya, V. I. Vasil'eva, P. Sistat, and G. Pourcelly, J. Membr. Sci. **447**, 190 (2013).
[12] E. A. Demekhin, N. V. Nikitin, and V. S. Shelistov, Phys. Fluids **25**, 122001 (2013).
[13] M. Z. Bazant, M. S. Kilic, B. D. Storey, and A. Ajdari, Adv. Colloid Interface Sci. **152**, 48 (2009).
[14] P. Mao and J. Han, Lab Chip **9**, 586 (2009).
[15] S. W. Nam, M. J. Rooks, K. B. Kim, and S. M. Rossnagel, Nano Lett. **9**, 2044 (2009).
[16] R. F. Probstein, *Physicochemical Hydrodynamics: An Introduction* (Wiley-Interscience, New York, 1994).
[17] Q. Pu, J. Yun, H. Temkin, and S. Liu, Nano Lett. **4**, 1099 (2004).
[18] S. J. Kim, L. Li, and J. Han, Langmuir **25**, 7759 (2009).
[19] S. J. Kim, Y.-C. Wang, J. H. Lee, H. Jang, and J. Han, Phys. Rev. Lett. **99**, 044501 (2007).
[20] G. Yossifon and H. C. Chang, Phys. Rev. E **81**, 066317 (2010).
[21] S. J. Kim, S. H. Ko, R. Kwak, J. D. Posner, K. H. Kang, and J. Han, Nanoscale **4**, 7406 (2012).
[22] S. M. Rubinstein, G. Manukyan, A. Staicu, I. Rubinstein, B. Zaltzman, R. G. H. Lammertink, F. Mugele, and M. Wessling, Phys. Rev. Lett. **101**, 236101 (2008).
[23] I. Rubinstein and B. Zaltzman, Phys. Rev. E **62**, 2238 (2000).
[24] G. Yossifon, P. Mushenheim, Y. C. Chang, and H. C. Chang, Phys. Rev. E **81**, 046301 (2010).
[25] Y.-C. Wang, A. L. Stevens, and J. Han, Anal. Chem. **77**, 4293 (2005).
[26] G. Yossifon, P. Mushenheim, and H. C. Chang, Europhys. Lett. **90**, 64004 (2010).
[27] A. Mani, T. A. Zangle, and J. G. Santiago, Langmuir **25**, 3898 (2009).
[28] A. Mani and M. Z. Bazant, Phys. Rev. E **84**, 061504 (2011).
[29] A. Yaroshchuk, Adv. Colloid Interface Sci. **183–184**, 68 (2012).
[30] E. V. Dydek and M. Z. Bazant, AIChE J. **59**, 3539 (2013).
[31] E. V. Dydek, B. Zaltzman, I. Rubinstein, D. S. Deng, A. Mani, and M. Z. Bazant, Phys. Rev. Lett. **107**, 118301 (2011).
[32] C. P. Nielsen and H. Bruus, Phys. Rev. E **90**, 043020 (2014).
[33] A. Yaroshchuk, E. Zholkovskiy, S. Pogodin, and V. Baulin, Langmuir **27**, 11710 (2011).
[34] I. Rubinstein and B. Zaltzman, J. Fluid Mech. **728**, 239 (2013).
[35] D. Deng, E. V. Dydek, J.-H. Han, S. Schlumpberger, A. Mani, B. Zaltzman, and M. Z. Bazant, Langmuir **29**, 16167 (2013).
[36] J.-H. Han, E. Khoo, P. Bai, and M. Z. Bazant, Sci. Rep. **4**, 7056 (2014).
[37] I. Cho, G. Sung, and S. J. Kim, Nanoscale **6**, 4620 (2014).
[38] A. A. Moya, E. Belashova, and P. Sistat, J. Membr. Sci. **474**, 215 (2015).
[39] See Supplemental Material at http://link.aps.org/supplemental/10.1103/PhysRevLett.114.114501 for details of experimental methods, videos showing transient electrokinetic flow patterns and additional experiment with varying the cross-sectional area of microchannel, which includes Refs. [26,37].
[40] R. Kwak, V. S. Pham, K. M. Lim, and J. Y. Han, Phys. Rev. Lett. **110**, 114501 (2013).
[41] R. A. Rica and M. Z. Bazant, Phys. Fluids **22**, 112109 (2010).